VIP Radiopharmacology Very Important Paper

DOI: 10.1002/ange.201303422

Positron Emission Tomography Imaging of Drug-Induced Tumor Apoptosis with a Caspase-Triggered Nanoaggregation Probe**

Bin Shen, Jongho Jeon, Mikael Palner, Deju Ye, Adam Shuhendler, Frederick T. Chin, and Jianghong Rao**

Positron emission tomography (PET) is a powerful noninvasive molecular imaging technique that uses molecules labeled with positron-emitting isotopes such as carbon-11, fluorine-18, and copper-64, to monitor biochemical processes in living subject in real time with excellent sensitivity.[1] A contrast-enhanced PET image is produced through selective retention of radioactivity at the location where the molecular target is present, and the common strategy is based on the binding of a radiolabeled ligand to the target receptor molecule. When the molecular target is an enzyme, the methods to generate PET imaging contrast are very few,[2] such as 2-[^{18}F]fluoro-2-deoxy-glucose ([^{18}F]FDG) for imaging hexokinase[3] and PET tracers for imaging herpes simplex virus-1 thymidine kinase.[4] Herein, we report a new strategy for developing PET tracers for imaging caspase-3 activity in tumors treated with doxorubicin.

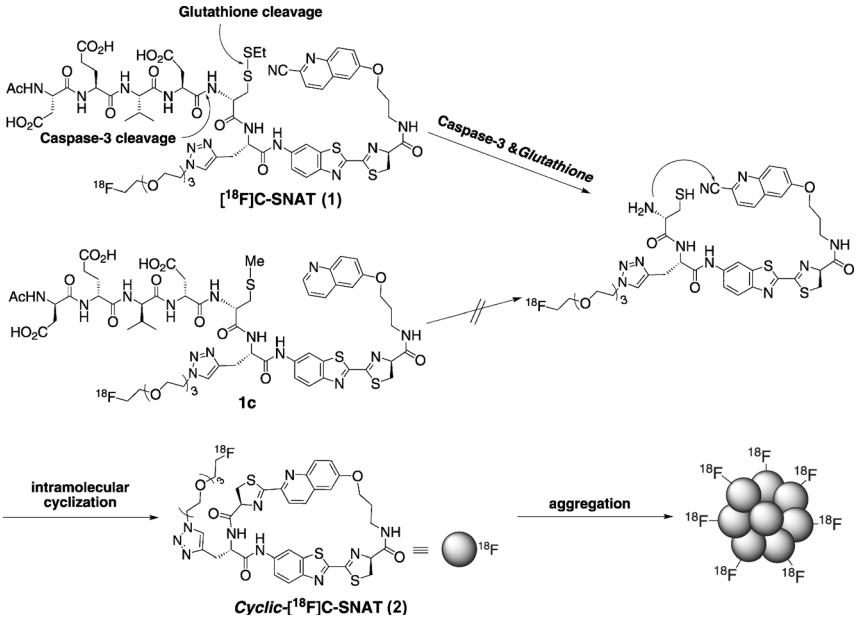

Scheme 1. Activation, intramolecular cyclization of [^{18}F]C-SNAT (**1**) and aggregation of cyclized product (**2**).

One of the most important pathways of chemotherapeutic-induced apoptosis leads to the activation of caspase-3, a central scavenging peptidase that cleaves a specific peptide sequence DEVD-X between X and D (where is X is any amino acid and DEVD is the amino acid sequence Asp-Glu-Val-Asp) committing the cell to programmed cell death—apoptosis.[5] While activatable fluorescent probes have been developed for imaging caspase-3 activity in cells and living mice,[6] there are only reports of radiolabeled caspase-3 inhibitors for PET imaging of caspase-3 in apoptotic cells.[7] There is not a general strategy to develop a PET tracer that is mechanistically similar to the activatable fluorescent probes in imaging caspase-3 activity with signal amplification.

We have previously described a biocompatible condensation reaction between 2-cyanobenzothiazole (CBT) and free cysteine for specific labeling of terminal cysteine residues in proteins[8] and controlled self-assembly of nanoaggregates in cells.[9] Herein, we applied it to develop PET tracers for imaging caspase activity, as outlined in Scheme 1. The ^{18}F-labeled caspase-sensitive nanoaggregation PET tracer ([^{18}F]C-SNAT, or **1**) has a 2-cyano-6-hydroxyquinoline (CHQ) and a cysteine residue, the amino group of which is coupled to the peptide substrate of caspase-3 or DEVD,[10] and the side-chain mercapto group of which is converted to a disulfide bond. The ^{18}F label is introduced to a propargylglycine residue between CHQ and the cysteine residue using the copper-catalyzed azide–alkyne 1,3-dipolar cyloaddition (CuAAC). Upon the activation of caspase-3 that cleaves the

[*] Dr. B. Shen,[+] Dr. J. Jeon,[+] Dr. M. Palner, Dr. D. Ye, Dr. A. Shuhendler, Prof. F. T. Chin, Prof. J. Rao
Department of Radiology
Molecular Imaging Program at Stanford
Stanford University School of Medicine
Stanford, CA 94305-5484 (USA)
E-mail: chinf@stanford.edu
jrao@stanford.edu

[+] These authors contributed equally to this work.

[**] This work has been supported by the Stanford University National Cancer Institute (NCI) Centers of Cancer Nanotechnology Excellence (grant number 1U54CA151459-01), the NCI ICMIC@Stanford (grant number 1P50CA114747-06), and an IDEA award from the Department of Defense Breast Cancer Research Program (grant number W81XWH-09-1-0057). M.P. is grateful to the postdoctoral fellowship support from the Danish Cancer Foundation, and A.S. is supported by a postdoctoral fellowship from the Susan Komen Breast Cancer Foundation. The use of Stanford Small Animal Imaging Facility is acknowledged.

Supporting information for this article is available on the WWW under http://dx.doi.org/10.1002/anie.201303422.

peptide DEVD, the amino group of the cysteine residue is released, and the reductive intracellular environment reduces the disulfide to generate a free thiol. As shown before,[11] free cysteine and CHQ can undergo fast intramolecular cyclization through the condensation reaction (half-life at 119.8 ± 10.2 s). The cyclized products are more hydrophobic and self-assemble in situ into nanoparticles with a high density of ^{18}F activity, resulting in prolonged retention in apoptotic cells and enhanced PET imaging contrast.

The control tracer **1D** is designed to have a similar structure and pharmacokinetics to **1** but cannot be cleaved by caspase-3 and undergo cyclization and aggregation. Therefore, it contains the same substrate sequence of caspase-3 but made of D-amino acids. In addition, **1D** does not have the cyano substitution on its quinoline and the mercapto group of the cysteine side chain is methylated.

The precursor **3a** for synthesizing **1** was prepared according to Scheme 2. *N*-Boc-propargylglycine was coupled with 6-amino-2-cyanobenzothiazole to afford **4**. Deprotection of the *N*-Boc group followed by coupling with protected D-cysteine provided the dipeptide **5**. Condensation of **5** and **6a** between the CBT group and cysteine under mild conditions, subsequent deprotection of *N*-Boc and *S*-trityl (*S*-Trt) groups and protection of the thiol group gave intermediate **7a**. The amino group of **7a** was coupled with the protected caspase-3 substrate, Ac-Asp(*t*Bu)-Glu(*t*Bu)-Val-Asp(*t*Bu)-OH **8a**, and final deprotection of the *tert*-butyl group gave the desired precursor **3a**. The precursor **3b** for the control PET tracer **1D** consisted of D-amino acids and was prepared similarly.

Both precursors were labeled with ^{18}F prosthetic group through CuAAC, as reported before[12] (Scheme 3). The prosthetic group **10** was obtained in a one-step substitution of **9** by ^{18}F ions in the presence of Kryptofix 222

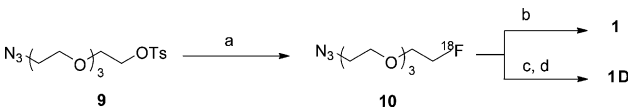

Scheme 3. Radiosynthesis of **1** and **1D**, a) ^{18}F/Kryptofix 222/K_2CO_3, DMSO, 110 °C, 20 minutes. b) **3a**, $Cu(CH_3CN)_4PF_6$, BPDS, DMSO/water, 60 °C, 30 minutes. c) **3b**, $CuSO_4$, sodium ascorbate, DMSO/water, 40 °C, 30 minutes. d) 3-Azidopropan-1-amine hydrochloride, 40 °C, 30 minutes. BPDS = bathophenanthrolinedisulfonic acid disodium salt trihydrate and DMSO = dimethyl sulfoxide.

(4,7,13,16,21,24-hexaoxa-1,10-diazabicyclo[8.8.8] hexacosane) with a radiochemical yield (RCY) of 37 ± 8 % ($n = 16$; decay corrected to end of bombardment, EOB). The CuAAC labeling of **3a** by **10** occurred under mild conditions (40–60 °C). When $CuSO_4$ and sodium ascorbate were employed, the RCY (EOB) in this step was 15 ± 6 % ($n = 6$) for **1** and 25 ± 8 % ($n = 4$) for **1D**. When $Cu(CH_3CN)_4PF_6$ and BPDS were applied, the RCY (EOB) increased to 30 ± 5 % ($n = 4$) for **1** with less side products, probably due to improved stability of **1** in the absent of sodium ascorbate. The final product was purified on a semi-preparative HPLC and formulated in saline containing < 10 % EtOH. During the HPLC purification of **1D**, because both the precursor **3b** and product **1D** had very close retention times ($\Delta t_R < 0.1$ min), 3-azidopropan-1-amine hydrochloride was added to convert remaining **3b** to a product with its retention time shifted to a much earlier time ($\Delta t_R >$ 10 min), which significantly improved the HPLC purification (Figure S1 in the Supporting Information). In summary, **1** and **1D** were successfully obtained with an overall RCY (decay corrected to end of synthesis, EOS) and specific radioactivity (EOS) of 3.2 ± 0.1 % and 63 ± 7.4 GBq μmol^{-1} (1.7 ± 0.2 Ci μmol^{-1}) for **1**, 1.8 ± 0.8 % and 99.9 ± 33.3 GBq μmol^{-1} (2.7 ± 0.9 Ci μmol^{-1}) for **1D** (radiochemical purity > 99 %, chemical purity > 95 %, Figure S2) after a total synthesis time of 3–3.5 h from EOB.

The serum stability of **1** and **1D** was tested in human and mouse serum. Both tracers showed > 90 % intact in human

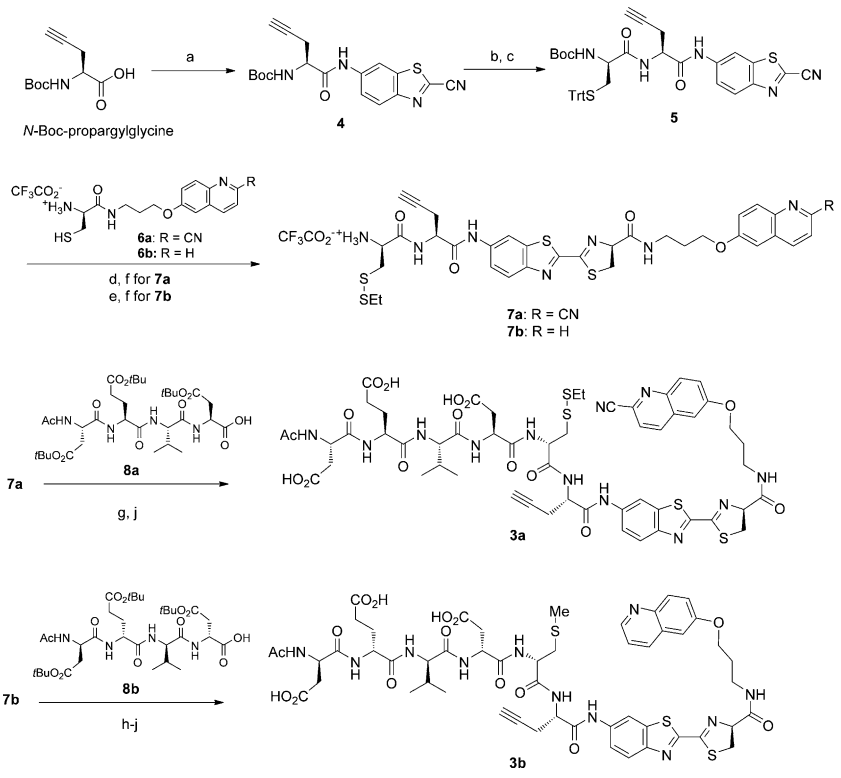

Scheme 2. Synthesis of precursors **3a** and **3b**. a) *iso*-Butyl chloroformate, 4-methylmorpholine, THF, 0 °C, 2 h and then 6-amino-2-cyanobenzothiazole, THF, 0 °C to RT, 12 h; 85 %. b) 60 % TFA in CH_2Cl_2, RT, 1 h. c) *N*-Boc-*S*-Trt-D-Cysteine, HBTU, DIPEA, DMF, RT, 2 h; 80 % from **4**. d) **6a**, DIPEA, DMF, RT, 30 min. e) **6b**, DIPEA, DMF, 30 min. f) 60 % TFA in CH_2Cl_2, RT, 1 h and then 2-(ethyldisulfanyl) pyridine, MeOH, RT, 2 h; 51 % from **5** for **7a**, 40 % for **7b**. g) Ac-DEVD-OH (**8a**), HBTU, DIPEA, THF, RT, 1 h. h) Ac-devd-OH (**8b**), HBTU, DIPEA, THF, RT, 1 h. i) CH_3I, TCEP·HCl, DIPEA, DMF, 1 h. j) 50 % TFA in CH_2Cl_2, RT, 2 h; 69 % (**3a**) from **7a**, 38 % (**3b**) from **7b**. TFA = trifluoroacetic acid, HBTU = *O*-(1*H*-benzotriazoyl-1-yl)-*N*,*N*,*N*′,*N*,′-tetramethyluronium hexafluorophosphate, DIPEA = diisopropylethylamine, Ac = acetyl, and TCEP·HCl = tris(2-carboxyethyl)phosphine hydrochloride.

serum after 2 h incubation at 37 °C. In mouse serum, **1D** displayed higher stability than **1**: 90 % of intact **1D** vs. 60 % of intact **1** was observed after 1 h incubation—probably due to the replacement by the D-amino acids. The cyclization product **2** was also tested and showed >90 % intact in mouse serum after 2 h incubation (Figure S3).

To evaluate the tracer **1** for caspase-3 detection, we first incubated it with recombinant caspase-3 in buffer. Within 1 h, 90 % of **1** was shown to cyclize and afford two cyclized isomers based on the radio-HPLC chromatograph (Figure 1 A).[13] As expected, under the same condition, **1D** could not be cleaved by caspase-3 and no cyclization product but **1D** itself was observed.

Next, we applied **1** to detect caspase-3 in apoptotic cells in vitro. HeLa cells were incubated with doxorubicin (Dox; 2 μM) for 24 h to induce apoptosis. Caspase-3 assays confirmed that the lysates of Dox-treated cells showed a 9.5-times higher caspase-3 activity than that of nontreated cells (Figure S4 A). Both Dox-treated and nontreated cells were then incubated with **1** for 4 h. The retained ^{18}F activity in Dox-treated cells was 2.2-times of that of nontreated cells. As control, a caspase-3 inhibitor (Z-VAD-fmk) was applied to a similar set of Dox-treated cells, which decreased the retained ^{18}F activity to 1.3-times (Figure 1 B). Both Dox-treated and nontreated cells were subject to extraction and analyzed by radio-HPLC. The major radioactive fractions from Dox-treated cells were cyclized products of **2** (Figure 1 A), but it was not observed in the extraction from non-Dox-treated cells. These results demonstrate that caspase-3 activity can trigger the cyclization of **1** in living cells and enhance the retention of the radioactivity.

The biodistribution of **1** was performed in nude mice that were euthanized at 120 minutes post tracer injection. Organs were collected, weighed, and analyzed with a gamma counter for radioactivity uptake (Table S1). Briefly, kidney and bladder showed high levels of absolute uptake, suggesting primary renal clearance of the tracer. A low tracer activity in the muscle promises a minimal background signal in PET imaging. Uptake in the brain was low, indicating that **1** could not cross the blood-brain barrier.

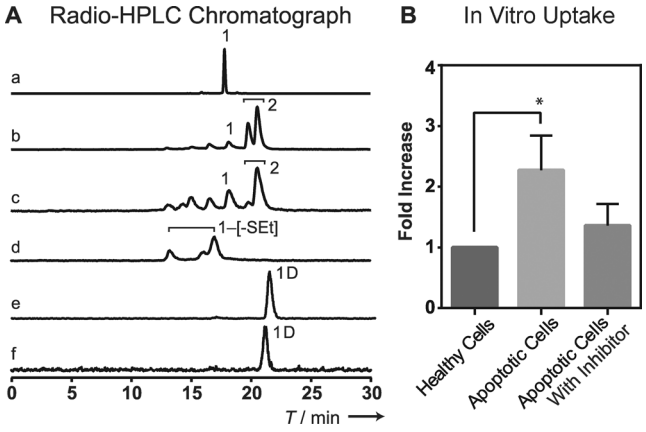

Figure 1. A) Analytical radio-HPLC showing the radioactive signal composition: a) **1** in saline; b) **1** incubated with caspase-3 in solution for 1 h; c) extraction from **1** cellular uptake in apoptotic cell (4 h); d) extraction from **1** cellular uptake in healthy cell (4 h). No cyclization product **2** but disulfide bond cleaved intermediates (**1**-[-SEt]) were observed in healthy cells. e) **1D** in saline; f) **1D** incubated with caspase-3 for 1 h. B) In vitro uptake (fold over healthy cell, $n=3$) of **1** in healthy HeLa cells, apoptotic HeLa cells (treated with 2 μM doxorubicin) and apoptotic HeLa cells with caspase-3 inhibitor (50 μM of Z-VAD-FMK) added. * indicates statistically significant $P=0.045$.

Evaluation of **1** and **1D** for PET imaging of caspase-3 activity in vivo was performed in HeLa tumor xenograft-bearing nude mice. The tumors were implanted and grown for more than 10 days before intratumoral injection of 0.2 mg Dox (20 μL). Four days post treatment, **1** or **1D** (5–15 MBq/135–405 μCi) were injected through the tail vein for PET imaging. Static PET scans (5 minutes) were performed 65, 125 and 182 minutes post tracer injection. Figure 2 shows representative PET images of the same mouse injected with **1** before and after Dox treatment and another mouse with **1D** after Dox treatment.

Quantification of the PET images with the activatable PET tracer **1** revealed that the percentage of the injected dose per gram tissue (%ID/g) of the ^{18}F activity in tumors significantly increased after Dox treatment: from 0.81 ± 0.28 (baseline) to 1.17 ± 0.17 (treated) at 65 minutes, and from 0.67 ± 0.24 (baseline) to 1.29 ± 0.07 (treated) at 182 minutes (Figure 3 A); this result correlates well with the caspase-3 level detected in tumors—a 1.9-fold increase in the treated tumors (Figure S4 B). The uptake difference between the baseline value and the value obtained for the treated tumors increased from 0.36 ± 0.15 at 65 minutes to 0.63 ± 0.11 at 182 minutes (Figure 3 B), and the uptake ratio between tumor and muscle (T/M) increased from 3.30-fold at 65 minutes to 7.00-fold at 182 minutes in treated tumors (Figure 3 C).

In contrast, the uptake of **1D** in both treated and nontreated tumors was much lower than that of **1** (Figure 3 A), and the uptake difference between before and after treatment (<0.2 %ID/g) was also much smaller (Figure 3 B). The ratio of T/M did not show significant increases either (Figure 3 C). Our PET imaging results demonstrate that **1** can image caspase-3 activity in drug-treated tumors in vivo and that both caspase-3 activation and cyclization are required for the enhanced imaging contrast in apoptotic tumors.

[^{18}F]C-SNAT (**1**) compares favorably to known apoptosis PET tracers (Table S2) with both a high tumor/muscle ratio in

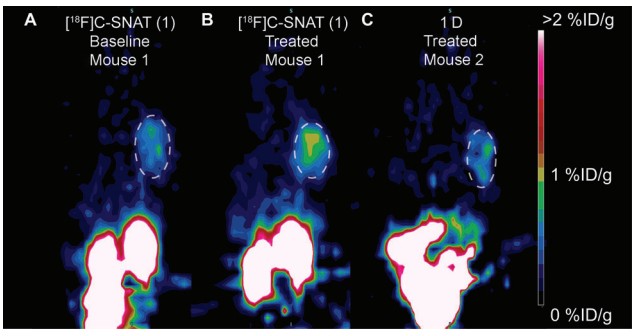

Figure 2. Representative PET images showing HeLa tumor xenografts (white dashed circles) on the right shoulder of mice 125 minutes after intravenous (i.v.) injection of the tracer A) before and B,C) after doxorubicin treatment. A) Mouse 1 before treatment imaged with **1** (7.8 MBq/211 μCi). B) Mouse 1 after treatment imaged with **1** (12 MBq/324 μCi). C) Mouse 2 after treatment imaged with **1D** (5.4 MBq/146 μCi). All images are normalized to the same scale.

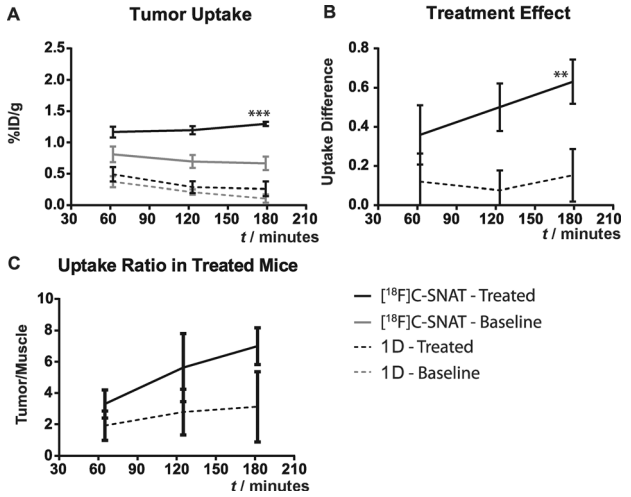

Figure 3. A) Uptake of **1** and **1D** (%ID/g ± sem) in a xenograft HeLa tumor and muscle, before and after intratumor injection of Dox (0.2 mg) 4 days prior to the imaging. The uptake is calculated based on 5 miniutes static PET scans at 65, 125 and 182 minutes. *** indicates $p = 0.002$ at 182 minutes. B) The uptake difference (%ID/g ± sem) of **1** (solid line) and **1D** (dashed line) between treated and untreated tumors; ** shows a significant $p = 0.0037$ at 182 minutes. C) The ratio between tumor and muscle uptake in treated tumors for **1** (solid line) and **1D** (dashed line), calculated based on the uptake (average uptake in tumor/average uptake in muscle region).

apoptotic tumors and a high uptake value (%ID/g) in apoptotic tumors. Consistent with the mechanism, [^{18}F]C-SNAT showed a trend of increasing uptake over time (Figure 3A) in apoptotic tumors and thus increased differences between treated apoptotic and nontreated tumors at later time points. This trend has not been observed with other apoptosis PET tracers; for example, with [^{18}F]ICMT-11, a PET tracer that binds active caspase-3, the uptake at the apoptotic tumors decreased over the time after tracer administration.[7a] Furthermore, our probe designing principle is not limited to caspase-3 but may serve as a general strategy for developing PET tracers for imaging the activity of other enzymes (i.e. furin, matrix metalloproteinases).

In conclusion, we have successfully designed and synthesized an ^{18}F-labeled caspase-3 triggered nanoaggregation PET tracer ([^{18}F]C-SNAT), and demonstrated its application for imaging caspase-3 activity in doxorubicin-treated tumor xenografts. This activatable PET tracer undergoes intramolecular cyclization and subsequent aggregation upon caspase-3 activation to achieve enhanced retention in apoptotic tumors. Applications of this strategy for other enzyme targets as well as translation of [^{18}F]C-SNAT into clinical studies are currently under investigation.

Received: April 23, 2013
Published online: July 23, 2013

Keywords: apoptosis · caspase-3 · cyclization · drug design · positron emission tomography

[1] a) E. J. Hoffman, M. E. Phelps, *Med. Instrum.* **1979**, *13*, 147–151; b) S. S. Gambhir, *Nat. Rev. Cancer* **2002**, *2*, 683–693.
[2] a) G. Ren, G. Blum, M. Verdoes, H. G. Liu, S. Syed, L. E. Edgington, O. Gheysens, Z. Miao, H. Jiang, S. S. Gambhir, M. Bogyo, Z. Cheng, *PLoS One* **2011**, *6*, e28029; b) A. Razgulin, N. Ma, J. Rao, *Chem. Soc. Rev.* **2011**, *40*, 4186–4216.
[3] a) T. Ido, C. N. Wan, V. Casella, J. S. Fowler, A. P. Wolf, M. Reivich, D. E. Kuhl, *J. Labelled Compd. Radiopharm.* **1978**, *14*, 175–183; b) J. Pacák, Z. Točik, M. Černy, *J. Chem. Soc. D* **1969**, 77.
[4] a) J. G. Tjuvajev, M. Doubrovin, T. Akhurst, S. Cai, J. Balatoni, M. Alauddin, R. Finn, P. Conti, J. G. Tjuvajev, R. Blasberg, *J. Nucl. Med.* **2002**, *43*, 1072–1083; b) M. Iyer, J. R. Barrio, M. Namavari, E. Bauer, N. Satyamurthy, K. Nguyen, T. Toyokuni, M. E. Phelps, H. R. Herschman, S. S. Gambhir, *J. Nucl. Med.* **2001**, *42*, 96–105; c) J. Tjuvajev, N. Avril, M. Safer, R. Joshi, T. Oku, T. Sasajima, T. Miyagawa, B. Beattie, F. Daghighian, F. Augenson, G. DiResta, J. Koutcher, J. Zweit, R. Finn, S. Larson, R. Blasberg, *J. Nucl. Med.* **1997**, *38*, 239p.
[5] a) J. A. Rosado, J. J. Lopez, E. Gomez-Arteta, P. C. Redondo, G. M. Salido, J. A. Pariente, *J. Cell. Physiol.* **2006**, *209*, 142–152; b) K. Schwarz, G. Simonis, X. J. Yu, S. Wiedemann, R. H. Strasser, *Mol. Cell. Biochem.* **2006**, *281*, 45–54; c) W. Lei, R. Yu, S. Mandlekar, A. N. T. Kong, *Cancer Res.* **1998**, *58*, 2102–2106.
[6] a) E. M. Barnett, X. Zhang, D. Maxwell, Q. Chang, D. Piwnica-Worms, *Proc. Natl. Acad. Sci. USA* **2009**, *106*, 9391–9396; b) L. E. Edgington, A. B. Berger, G. Blum, V. E. Albrow, M. G. Paulick, N. Lineberry, M. Bogyo, *Nat. Med.* **2009**, *15*, 967–974; c) Z. Zhang, J. Fan, P. P. Cheney, M. Y. Berezin, W. B. Edwards, W. J. Akers, D. Shen, K. Liang, J. P. Culver, S. Achilefu, *Mol. Pharm.* **2009**, *6*, 416–427.
[7] a) Q. D. Nguyen, G. Smith, M. Glaser, M. Perumal, E. Arstad, E. O. Aboagye, *Proc. Natl. Acad. Sci. USA* **2009**, *106*, 16375–16380; b) D. Zhou, W. H. Chu, D. L. Chen, Q. Wang, D. E. Reichert, J. Rothfuss, A. D'Avignon, M. J. Welch, R. H. Mach, *Org. Biomol. Chem.* **2009**, *7*, 1337–1348; c) A. Faust, S. Wagner, M. P. Law, S. Hermann, U. Schnockel, P. Keul, O. Schober, M. Schafers, B. Levkau, K. Kopka, *Q. J. Nucl. Med. Mol. Imaging* **2007**, *51*, 67–73; d) A. Reshef, A. Shirvan, A. Akselrod-Ballin, A. Wall, I. Ziv, *J. Nucl. Med.* **2010**, *51*, 837–840; e) C. Xia, G. Chen, U. Gangadharmath, L. F. Gomez, Q. Liang, F. R. Mu, V. P. Mocharla, H. Su, A. K. Szardenings, J. C. Walsh, T. Zhao, H. C. Kolb, *Mol. Imaging. Biol.* **2013**, DOI: 10.1007s11307-013-0644-9.
[8] a) H. J. Ren, F. Xiao, K. Zhan, Y. P. Kim, H. X. Xie, Z. Y. Xia, J. Rao, *Angew. Chem.* **2009**, *121*, 9838–9842; *Angew. Chem. Int. Ed.* **2009**, *48*, 9658–9662; b) J. Jeon, B. Shen, L. Q. Xiong, Z. Miao, K. H. Lee, J. Rao, F. T. Chin, *Bioconjugate Chem.* **2012**, *23*, 1902–1908.
[9] a) G. L. Liang, H. J. Ren, J. Rao, *Nat. Chem.* **2010**, *2*, 54–60; b) G. L. Liang, J. Ronald, Y. X. Chen, D. J. Ye, P. Pandit, M. L. Ma, B. Rutt, J. Rao, *Angew. Chem.* **2011**, *123*, 6407–6410; *Angew. Chem. Int. Ed.* **2011**, *50*, 6283–6286.
[10] Caspase-7, another effector caspase can aslo recognize this peptide sequence.
[11] D. J. Ye, G. L. Liang, M. L. Ma, J. Rao, *Angew. Chem.* **2011**, *123*, 2323–2327; *Angew. Chem. Int. Ed.* **2011**, *50*, 2275–2279.
[12] a) C. Mamat, T. Ramenda, F. R. Wuest, *Mini-Rev. Org. Chem.* **2009**, *6*, 21–34; b) H. S. Gill, J. Marik, *Nat. Protoc.* **2011**, *6*, 1718–1725; c) K. Nwe, M. W. Brechbiel, *Cancer Biother. Radiopharm.* **2009**, *24*, 289–302; d) M. Glaser, E. G. Robins, *J. Labelled Compd. Radiopharm.* **2009**, *52*, 407–414.
[13] Two cyclized isomers are likely diastereomers because of two different ring-closing orientations, as observed in our previous study (Ref. [11]).